The Plant Cell, Vol. 15, 2826–2842, December 2003, www.plantcell.org © 2003 American Society of Plant Biologists

A Class-V Myosin Required for Mating, Hyphal Growth, and Pathogenicity in the Dimorphic Plant Pathogen *Ustilago maydis* [W]

Isabella Weber, Christian Gruber,[1] and Gero Steinberg[2]

Max-Planck-Institut für Terrestrische Mikrobiologie, D-35043 Marburg, Germany

In the early stages of plant infection, yeast-like haploid sporidia of *Ustilago maydis* respond to pheromone secreted by compatible partners by forming conjugation tubes. These then fuse to generate a dikaryotic hypha that forms appressoria to penetrate the host plant. As a first step toward understanding the structural requirements for these transitions, we have identified *myo5*, which encodes a class-V myosin. Analysis of conditional and null mutants revealed that Myo5 plays nonessential roles in cytokinesis and morphogenesis in sporidia and is required for hyphal morphology. Consistent with a role in morphogenesis, a functional green fluorescent protein–Myo5 fusion protein localized to the bud tip and the hyphal apex as well as to the septa and the spore wall during later stages of infection. However, the loss of Myo5 did not affect the tip growth of hyphae and sporidia. By contrast, Myo5 was indispensable for conjugation tube formation. Furthermore, *myo5* mutants were impaired in the perception of pheromones, which indicates a particular importance of Myo5 in the mating process. Consequently, few mutant hyphae were formed that penetrated the plant epidermis but did not continue invasive growth. These results indicate a crucial role of Myo5 in the morphogenesis, dimorphic switch, and pathogenicity of *U. maydis*.

INTRODUCTION

The smut fungus *Ustilago maydis* is a dimorphic pathogen of maize that infects its host plant only in the dikaryotic stage of its life cycle (Christensen, 1963). The pathogenic development starts when two haploid yeast–like sporidia of opposite mating type recognize each other on the plant surface. The key regulators of pathogenic development are encoded by the *a* and *b* mating loci (Banuett, 1995; Kahmann et al., 1995). The *a* locus encodes a pheromone lipopeptide/receptor system, whereas the *b* locus provides for two subunits of a transcription factor (Bölker et al., 1992; Gillissen et al., 1992). After stimulation of the cell by pheromones of the mating partner, the expression of endogenous *mating pheromone* (*mfa*) genes is upregulated (Urban et al., 1996) and cell cycle arrest is initiated (Garcia-Muse et al., 2003). Subsequently, haploid yeast–like sporidia undergo a morphological switch to hyphal growth and form conjugation tubes that extend toward the pheromone source (Spellig et al., 1994; Snetselaar et al., 1996). After fusion of two cells, compatible products of the *b* alleles dimerize in the common cytoplasm of the resulting dikaryon, and this *b* heterodimer transcriptionally controls subsequent pathogenic development (Kahmann et al., 1995; Kämper et al., 1995). The dikaryotic hypha continues tip growth until it penetrates the host epidermis by the formation of an appressorium-like structure. Finally, the fungus invades the plant and induces the formation of tumors in which the pathogenic cycle is completed by the development of diploid spores.

Although the switch from yeast to a tip-growing hypha is of central importance for pathogenicity, little is known about the mechanistic details and structural requirements for this morphological transition. In tip-growing plant cells (Hepler et al., 2001) and fungal hyphae (Heath, 1995), apical extension is based on the intracellular transport of vesicles and growth supplies along the cytoskeleton. Numerous studies indicate a role for both microtubules and F-actin in hyphal growth (Heath, 1995), and the recent identification and characterization of microtubule-based kinesin and dynein motors in fungal hyphae illustrate the importance of the tubulin cytoskeleton in the growth of fungal hyphae (Plamann et al., 1994; Steinberg and Schliwa, 1995; Xiang et al., 1995; Seiler et al., 1997; Steinberg et al., 1998; for overview, see Steinberg, 2000). By contrast, little is known about the role of myosin motors in filamentous fungi. The best-characterized myosin is MyoA, a class-I myosin from *Aspergillus nidulans* (McGoldrick et al., 1995), which is involved in endocytosis and hyphal morphogenesis (Osherov et al., 1998; Yamashita and May, 1998). Such a role of class-I myosins in the formation of hyphae was confirmed recently in *Candida albicans* (Oberholzer et al., 2002). However, studies with *Saccharomyces cerevisiae* and *Schizosaccaromyces pombe* demonstrate that class-V myosins are major organelle transporters that mediate secretory vesicle delivery and morphogenesis (Govindan et al., 1995; Karpova et al., 2000; Motegi et al., 2001; Win et al., 2001). Moreover, deletion mutants in a *C. albicans* class-V myosin are unable to grow filamentously (Woo et al., 2003), suggesting that class-V myosins are good candidates for the actin-based transport machinery underlying hyphal growth and dimorphic transition in filamentous and dimorphic fungi.

[1] Current address: Biomax Informatics AG, Lochhamer Strasse 11, D-82152 Martinsried, Germany.

[2] To whom correspondence should be addressed. E-mail gero.steinberg@staff.uni-marburg.de; fax 49-6421-178-509.

[W] Online version contains Web-only data.

Article, publication date, and citation information can be found at www.plantcell.org/cgi/doi/10.1105/tpc.016246.

Here, we describe the identification and characterization of Myo5, a motor protein of the unconventional class-V myosin family in *U. maydis*. We provide evidence that this myosin accumulates at the tips of sporidia and hyphae and shows properties characteristic of myosin motors. Using deletion and conditional mutants, we show that Myo5 is required at all morphological stages of *U. maydis*, including yeast-like sporidia, conjugation tubes, and dikaryotic hyphae.

RESULTS

U. maydis Contains a Single Class-V Myosin

As a first step toward understanding the role of myosins in the pathogenic development of *U. maydis*, we used degenerate primers to amplify conserved regions within the motor domains of class-V myosins. Subcloning and sequencing revealed an open reading frame of 4833 bp whose predicted motor domain is most similar to members of the class V unconventional myosin family (Figure 1A). This gene was designated *myo5*. The predicted protein product of *myo5*, Myo5, comprises 1611 amino acids and shares 47 to 64% identity in its motor region and 17 to 32% identity in its neck and tail regions with class-V myosins from yeast and vertebrates. Myo5 shares high sequence identity with Myo2p from *S. cerevisiae* (42% overall identity; Figure 1B) and with Myo52/Myo4 from *S. pombe* (34% overall identity). Alignment of Myo5 with these class-V myosins and Myo5A from mouse demonstrates that Myo5 shares a similar domain structure (Figure 1C).

The C-terminal tail of Myo5 is predicted to contain the conserved AF-6/CNO homology domain (E value of $4e^{-401}$; Pfam) that is implicated in the interaction between class-V myosins and a conventional kinesin (Huang et al., 1999). Myo5 contains six tandem IQ motifs (E values of 6.7 e^{-4} to 7.6 e^{-05}; Pfam) that are known to be required for light chain and calmodulin binding in Myo2p (Shannon and Li, 2000, and references therein), as well as conserved residues in the C terminus that correspond to secretory and vacuolar functions of Myo2p

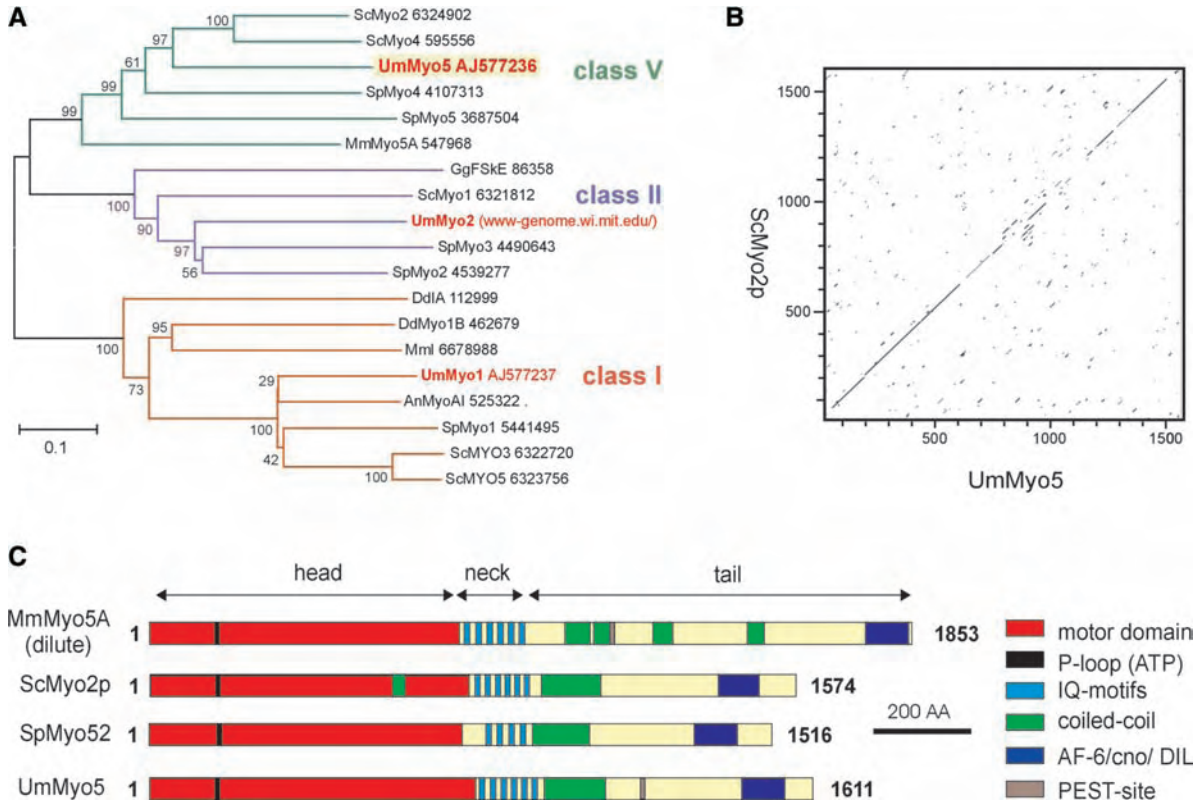

Figure 1. Myo5 Is a Class-V Myosin.

(A) A dendrogram of myosins created by the distance-based minimum-evolution method, based on 500 replicates. Note that *U. maydis* contains one myosin of class V, I, and II. Bootstrap values are given, and branching points and the scale bar denote substitutions per site. Sc, *Saccharomyces cerevisiae*; Um, *Ustilago maydis*; Sp, *Schizosaccharomyces pombe*; Mm, *Mus musculus*; Gg, *Gallus gallus*; Dd, *Dictyostelium discoideum*; An, *Aspergillus nidulans*.

(B) Dot plot comparison of Myo5 and Myo2p from *S. cerevisiae*. Note that both motors share significant sequence identity over the entire length.

(C) Comparison of the domain structures of Myo5 and Myo2p from *S. cerevisiae*, Myo52/Myo4 of *S. pombe*, and mouse Myo5A. Myo5 contains all predicted domains that are typical for class-V myosins. AA, amino acids.

(Catlett and Weisman, 1998; Schott et al., 1999). Unlike Myo2p and Myo52/Myo4, Myo5 contains a conserved Ser residue in its tail region (Ser-1405) that mediates the cargo release of *Xenopus* Myo5 via calcium-dependent phosphorylation (Karcher et al., 2001) and a putative PEST site (amino acids 1198 to 1215; PESTfind) that is implicated in calcium-regulated proteolysis (Rechsteiner, 1990). While this study was being completed, the genome of *U. maydis* was sequenced and published by the Whitehead Institute and Bayer Crop Science (for URL, see Methods). Screening of the genomic sequence revealed that *myo5* is the only class-V myosin in *U. maydis*.

myo5 Is Nonessential but Required for Normal Morphogenesis and Cell Separation

To analyze the function of Myo5, a deletion strain was generated by gene replacement in the haploid strain FB2 (*a2b2*) (for strains, see Table 1). The absence of *myo5* in the null mutant FB2ΔMyo5 was confirmed by DNA and RNA gel blot analyses (data not shown). Similar to mutants in *myo52*$^+$/*myo4*$^+$ from *S. pombe* (Motegi et al., 2001; Win et al., 2001), Δ*myo5* cells were viable but grew slowly (Figure 2A; the doubling time in liquid culture of control strain FB2 was 2.01 h at 28°C, and that in FB2ΔMyo5 was 6.48 h at 28°C). In contrast to the characteristic elongated, cigar-shaped wild-type morphology (Figure 2B1), Δ*myo5* cells were much thicker and usually failed to separate, thereby forming large cell aggregates that were divided by septa (Figure 2B2, arrow). Cells at the periphery of these aggregates still were elongated (Figure 2B3, arrowhead), suggesting that they were able to undergo polarized growth, whereas older Δ*myo5* cells often lost polarity and became almost spherical (Figure 2B3, arrow). The ability to grow in a polar manner also was reflected by the polar organization of F-actin patches at apical growth sites (Figure 2C; anti-actin antibodies) and by caps of newly deposited chitin at these tips (Figure 2D; wheat germ agglutinin [WGA] staining). This distribution of chitin coincided with the polar localization of chitin synthases that was detected with a broadly cross-reactive anti-Chs2p antibody (Sietsma et al., 1996; kindly provided by H. Sietsma [University of Groningen, Haren, The Netherlands] and H. Deising [Martin-Luther-University, Halle, Germany]) (Figure 2E).

To gain further insight into the role of Myo5 in polar growth, we introduced a temperature-sensitive mutant allele (*myo5*^{ts}) in the null mutant that contained a point mutation (E534K) in the motor domain that confers temperature sensitivity to Myo2p in *S. cerevisiae* (Lillie and Brown, 1994). At the permissive temperature (20°C), *myo5*^{ts} mutants grew slightly slower (Figure 2A) and were thicker, but they did grow by polar budding and

Table 1. Strains and Plasmids Used in This Study

Strains/Plasmids	Genotype	Reference
FB1	*a1b1*	Banuett and Herskowitz, 1989
FB2	*a2b2*	Banuett and Herskowitz, 1989
FB2ΔMyo5	*a2b2* Δ*myo5::hyg*^{R}	This study
FB2Myo5^{ts}	*a2b2* Δ*myo5::hyg*^{R}/pMyo5^{ts}	This study
FB2mGM	*a2b2* Δ*myo5::hyg*^{R}/pOGmyo5C	This study
FB2oGM	*a2b2* Δ*myo5::hyg*^{R}/pOGmyo5C	This study
AB33	*a2 bE2* Δ[*b2*^{I}, bW2^V]::[P*nar, ble*^{R}, nar(p), bW1^V]	Brachmann et al., 2001
AB33oGM	*a2 bE2* Δ[*b2*^{I}, bW2^V]::[P*nar, ble*^{R}, nar(p), bW1^V]/pOGmyo5C	This study
GS1Myo5^{ts}	*a1b1* Δ*myo5::hyg*^{R}/pMyo5ts	This study
GS2mGM	*a1b1* Δ*myo5::hyg*^{R}/pMGmyo5	This study
FB1Y	*a1b1*/pOY	This study
FB2C	*a2b2*/pOC	This study
FB2Myo5^{ts}C	*a2b2* Δ*myo5::hyg*^{R}/pMyo5^{ts} /pOC	This study
GS1Myo5^{ts}Y	*a1b1* Δ*myo5::hyg*^{R}/pMyo5^{ts} /pOY	This study
FB2mG	*a2b2*/pmfa1GFP	Spellig et al., 1996
FB1mG	*a1b1*/pmfa1GFP	Spellig et al., 1996
FB2Myo5^{ts}mG	*a2b2* Δ*myo5::hyg*^{R}/pMyo5^{ts}/pmfa1GFP	This study
GS1Myo5^{ts}mG	*a1b1* Δ*myo5::hyg*^{R}/pMyo5^{ts}/pmfa1GFP	This study
SG200	*a1mfa2bW2bE1, ble*^{R}	Bölker et al., 1995
SG200ΔKin2	*a1mfa2bW2bE1* Δ*kin2::cbx*^{R}, ble^R	Wedlich-Söldner et al., 2000
SG200ΔKin2oGM	*a1mfa2bW2bE1* Δ*kin2::cbx*^{R}, ble^R/pOGmyo5H	This study
pMyo5^{ts}	P*myo5-myo5*$_{E534K}$, cbx^R	This study
pMGmyo5	P*myo5-egfp-myo5, cbx*^{R}	This study
pOGmyo5C	P*otef-egfp-myo5, cbx*^{R}	This study
pOGmyo5H	P*otef-egfp-myo5, hyg*^{R}	This study
pOY	P*otef-yfp*, *ble*^{R}	This study
pOC	P*otef-cfp*, *ble*^{R}	This study
pmfa1GFP	P*mfa1-egfp*,*ble*^{R}	This study

a and *b*, mating-type loci; Δ, deletion; P, promoter; *::*, homologous replacement; -, fusion; ^{ts}, temperature-sensitive allele; *hph*^{R}, hygromycin resistance; *ble*^{R}, phleomycin resistance; *cbx*^{R}, carboxin resistance; /, ectopically integrated; *E2*, *W2*, and *W1*, genes within the *b* mating-type locus; ^{I}, intergenic region of the *b* locus; ^{V}, variable region of *b* genes*; egfp*, enhanced green fluorescent protein; *E534K*, point mutation at amino acid 534.

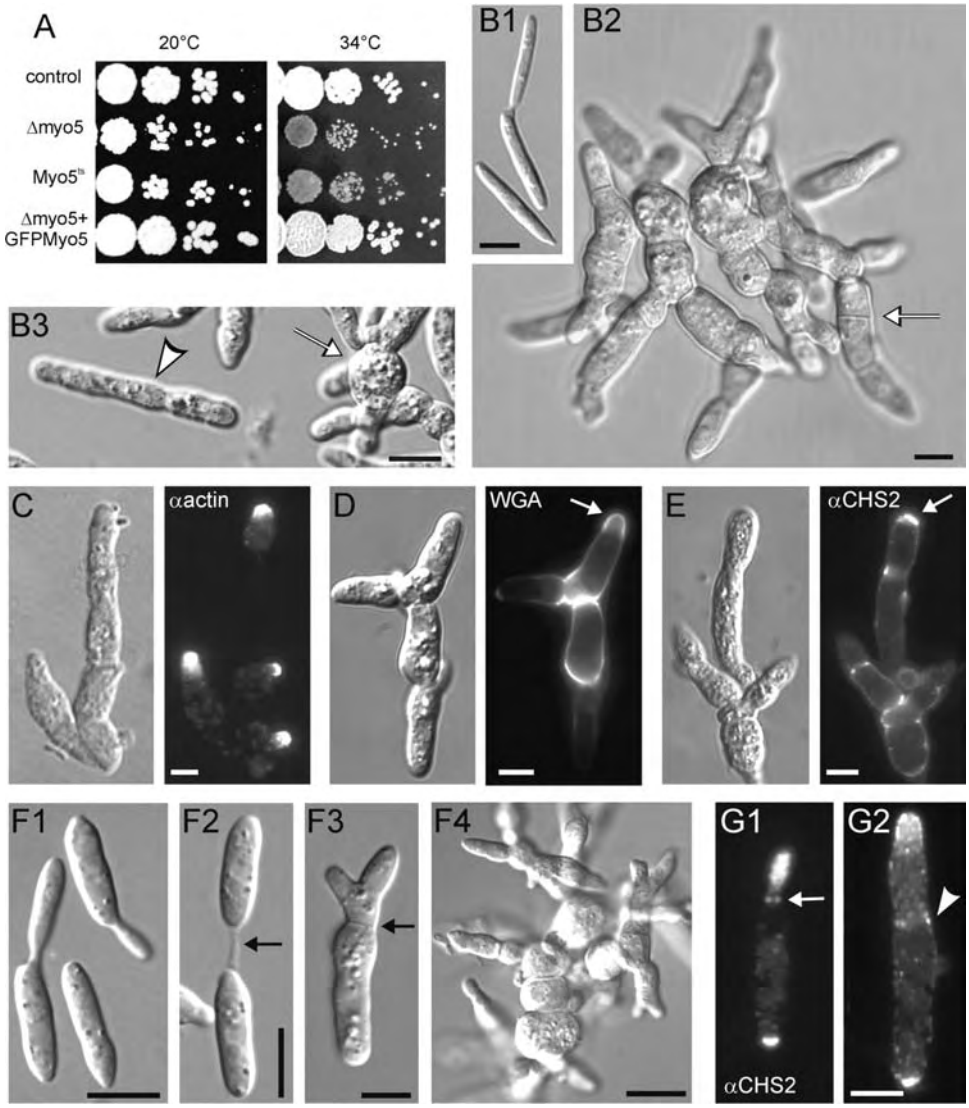

Figure 2. Characterization of Δ*myo5* and Temperature-Sensitive *myo5*^{ts} Mutants.

(A) Plate growth of FB2 (control) and myosin mutants at 20 and 34°C. At low temperature, the growth of control cells, Δ*myo5*, and *myo5*^{ts} is indistinguishable. However, both Δ*myo5* and *myo5*^{ts} show growth defects at 34°C that can be rescued by the expression of a functional GFP-Myo5 fusion protein. Note that *myo5* is not essential for the survival of *U. maydis*.

(B) Morphology defect of Δ*myo5* cells. Wild-type cells are cigar shaped and form polar buds (**[B1]**). By contrast, deletion of *myo5* leads to very thick and irregularly shaped cell aggregates. Most cells do not separate but form septa (arrow in **[B2]**). Interestingly, most Δ*myo5* cells are elongated (arrowhead in **[B3]**), whereas older cells often lose polarity and are rounded (arrow in **[B3]**). Bars = 5 μm.

(C) Polar distribution of F-actin patches in Δ*myo5* stained with anti-actin antibodies. Bar = 5 μm.

(D) Chitin distribution in Δ*myo5*. Rhodamine-labeled wheat germ agglutinin (WGA) detects newly synthesized chitin at cell tips (arrow), indicating that Δ*myo5* mutants grow in a polar manner. Bar = 5 μm.

(E) Localization of chitin synthase detected with a cross-reactive antibody raised against Chs2p from *S. cerevisiae* (Sietsma et al., 1996) in Δ*myo5* mutants. The antibody most likely detects chitin synthases at the growing tip of Δ*myo5* cells, in agreement with the WGA staining of chitin. Bar = 5 μm.

(F) Morphology of temperature-sensitive *myo5*^{ts} mutants. At the permissive temperature (20°C, **[F1]**), FB2Myo5^{ts} strains grow by polar budding but are significantly thicker than control cells (see **[B1]** for comparison). At the restrictive temperature (34°C), mutant cells show a defect in dissolving the cell wall after cytokinesis (arrow in **[F2]**; 1.5 h at 34°C). At later stages at 34°C, they form septa (arrow in **[F3]**; 6 h at 34°C) and start branching. After extended growth at 34°C, *myo5*^{ts} mutants form large aggregates that are reminiscent of Δ*myo5* cells. Bars = 5 μm in **(F1)** to **(F3)** and 10 μm in **(F4)**.

(G) Chitin synthase distribution in *myo5*^{ts} cells. At the permissive temperature, anti-Chs2p antibodies detect punctate staining in the growing bud, a ring at the bud neck (arrow in **[G1]**), and the distal cell pole. At 34°C, this chitin synthase distribution is largely unaffected, although more anti-Chs2p signals are detected at the periphery (arrowhead in **[G2]**). Note that the distribution of anti-Chs2p signals is very much in agreement with chitin staining (not shown) and the expected localization of chitin syntheses at the growth region, suggesting that the cross-reactive antibody is specific for chitin synthase in *U. maydis*. Bar = 5 μm.

showed no cytokinesis defect (Figure 2F1; for comparison, see control in Figure 2B1). After a shift to restrictive conditions (34°C), cells enlarged further and exhibited the first defects in cell separation, with fine wall fibers connecting the almost separated cells (Figure 2F2, arrow; 1.5 h at 34°C). Prolonged time at 34°C resulted in branching and septum formation (Figure 2F3, arrow; 6 h at 34°C), finally leading to large aggregates consisting of elongated and apolar cells that were reminiscent of those seen in Δ*myo5* mutants (Figure 2F4; for comparison, see Figure 2B2). In *myo5*^{ts} mutants in permissive conditions, the anti-Chs2p antibody detected putative chitin synthases in the growing bud, at the bud neck (Figure 2G1, arrow), and at the opposite cell pole, where the bud scar is located. This pattern also was typical for wild-type control cells (data not shown). After growth at 34°C for 6 h, chitin synthases localized at the cell periphery (Figure 2G2, arrowhead) and concentrated at the growing tip and the distal bud scar. In addition, F-actin and WGA were found to be concentrated at the growing tip of *myo5*^{ts} cells after 3 to 6 h at 34°C (data not shown), again indicating that *myo5* mutants are able to grow in a polar manner. In summary, these data show that Myo5 is required for cell separation and proper morphogenesis but not for polar actin and chitin synthase organization or the polarity of newly formed cells.

Localization of GFP-Myo5 to Sites of Exocytosis Depends on F-Actin

To further elucidate the cellular role of Myo5, we constructed an N-terminal GFP-Myo5 fusion protein. GFP-Myo5 expressed under its native *myo5* promoter fully rescued the growth and morphology phenotype of Δ*myo5* (Figures 2A and 3A). In apolar unbudded cells, the fusion protein was distributed randomly at the cell periphery (Figure 3A1) but accumulated at one cell pole before bud emergence (Figure 3A2). During early budding, a single GFP-Myo5 dot was observed at the bud tip (Figure 3A3). This region is characterized by the depositioning of newly synthesized chitin (Wedlich-Söldner et al., 2002), suggesting that GFP-Myo5 localizes to sites of exocytosis. Interestingly, cells with medium-sized buds often contained an additional GFP-Myo5 signal at the rear cell pole, suggesting exocytic activity at this cell end (Figure 3A4, arrow). Finally, GFP-Myo5 concentrated at the cleavage site (Figure 3A5, arrow), where it most likely participates in septum formation or cell separation (compared with Figure 2F2).

We analyzed the relationship of GFP-Myo5 distribution and F-actin by immunostaining of actin in gently fixed GFP-Myo5 cells. During most stages of polar growth, the fusion protein colocalized with actin patches (Figure 3B), but both signals separated in G1 when actin was recruited to the cleavage site (Figures 3B4 and 3B5, arrows), indicating that Myo5 is not a component of actin patches. Finally, GFP-Myo5 also accumulated at the neck region and colocalized with F-actin (Figure 3B6). In FB2oGM, which expresses GFP-Myo5 under the strong *otef* promoter (Spellig et al., 1996), oxygen depletion caused by prolonged observation resulted in the appearance of filamentous structures (Figure 3C) that were reminiscent of F-actin cables described for *U. maydis* (Banuett and Herskowitz, 2002). This effect of anoxia could be reproduced by treatment with carbonyl cyanide *m*-chlorophenylhydrazone (CCCP; Figures 3D1 and 3D2), which rapidly depletes ATP from the cytosol (Azarkina and Konstantinov, 2002). The CCCP-induced filaments were sensitive to the actin inhibitor cytochalasin D (Figure 3D3), suggesting that they are F-actin cables decorated with tightly bound GFP-Myo5. An interaction of GFP-Myo5 was further indicated by the fact that the polar accumulation of the fusion protein in the bud tip was insensitive to the disruption of microtubules by 20 μM benomyl but disappeared after the inhibition of F-actin with 50 μM latrunculin A or the inhibition of myosin activity with 10 mM 2,3-butanedione monoxime (BDM; Figures 3E1 to 3E3). In general, GFP-Myo5 signals were not mobile, but motility was found after prolonged exposure to light during microscopic observation, which disintegrated the apical GFP-Myo5 accumulation and induced the directed motion of GFP-Myo5 (see supplemental data online).

On charcoal-containing agar plates, two haploid-compatible cells fused to give rise to a dikaryotic hypha. In hypha from a cross of FB1 × FB2mG, the fusion protein GFP-Myo5 concentrated at the hyphal apex, but no signal was detected at the septum (Figure 4A, arrows). The apical GFP-Myo5 signal in dikaryotic hyphae was quite variable, ranging from a concentrated dot at the tip to dispersed gradients and long GFP-Myo5–decorated filaments (data not shown), suggesting that the GFP-Myo5 localization is very sensitive to experimental conditions. To circumvent this problem, we expressed GFP-Myo5 in strain AB33oGM, which contains compatible *bE1* and *bW2* genes under the control of inducible promoters, allowing the induction of hyphal growth in liquid culture by changing growth conditions (Brachmann et al., 2001). In these hyphae, GFP-Myo5 concentrated in a single focused dot at the apex (Figure 4B), suggesting that the dispersed gradient seen in most dikaryotic hyphae from plates is an artifact.

Consistent with the results obtained in haploid sporidia, the tip localization in hyphae was strongly dependent on intact F-actin and myosin activity, because the apical signal disappeared in 50 μM latrunculin and was reduced strongly in 10 mM BDM (Figures 4C1, 4C3, 4C4, and 4D). Benomyl treatment (20 μM) did not abolish apical GFP-Myo5 accumulation but resulted in a dispersed gradient of the fusion protein (Figures 4C2 and 4D), suggesting that microtubule-based transport participates in focusing GFP-Myo5 at the hyphal tip. In higher eukaryotes, evidence exists for an interaction of myosin V and conventional kinesin (Huang et al., 1999). *U. maydis* contains a conventional kinesin (Kin2; Lehmler et al., 1997), and we considered it possible that Kin2 supports GFP-Myo5 transport in *U. maydis*. Consequently, we generated a hyphal-growing *kin2* null strain that expressed GFP-Myo5. This strain showed the impaired filamentation typical for Δ*kin2* mutants (Figure 4E1) (Lehmler et al., 1997). However, in Δ*kin2* hyphae, GFP-Myo5 still was focused at the tip (Figure 4E2), which does not support a role of this kinesin in GFP-Myo5 organization.

myo5^{ts} Mutants Show Reduced Dikaryon Formation That Is Attributable to Impaired Pheromone Perception and Conjugation Tube Formation

To gain insights into the role of Myo5 in hyphal growth, we crossed compatible wild-type and *myo5* mutant strains on

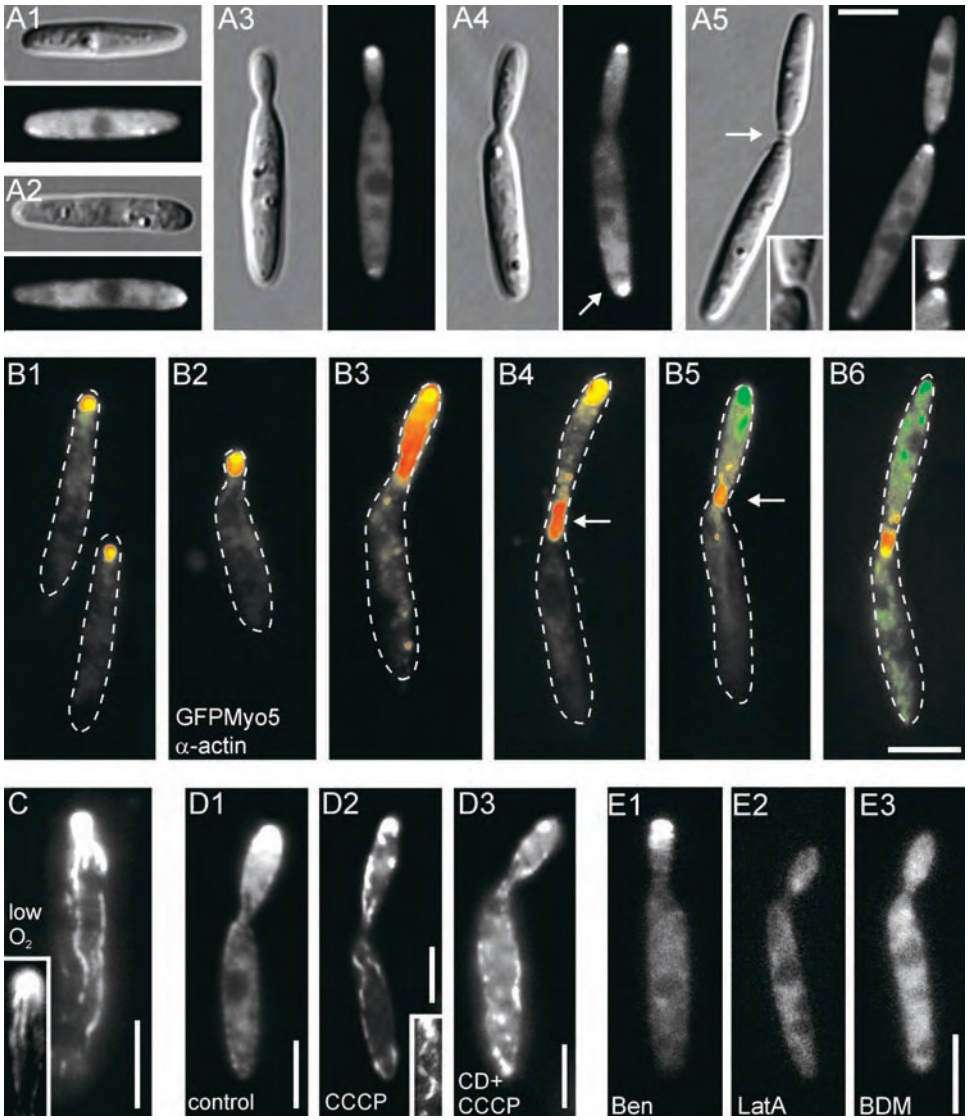

Figure 3. Localization of a Functional GFP-Myo5 Fusion Protein in Haploid Sporidia.

(A) GFP-Myo5 distribution during stages of the cell cycle. GFP-Myo5, expressed under the control of its native promoter, rescues the phenotype of Δ*myo5* cells. In presumably nongrowing cells, GFP-Myo5 shows a dispersed localization at the cell periphery **(A1)**. Before bud formation, cells begin to polarize and GFP-Myo5 concentrates at one cell pole **(A2)**. In small-budded cells, GFP-Myo5 remains at the bud tip **(A3)**, whereas in cells with medium-sized buds, the fusion protein localizes to the growing and the nongrowing ends of the cell (arrow in **[A4]**). Finally, it accumulates at the site of cell cleavage (**[A5]**; inset shows the equal signal intensity on both sides of the formed septa). Note that the distal localization of GFP-Myo5 (arrow in **[A4]**) coincides with the appearance of endosomes at this cell pole (Wedlich-Söldner et al., 2000, 2002), which suggests exocytotic activity at this cell end. Bar = 5 μm.

(B) Distribution of GFP-Myo5 and immunolabeled actin patches during the cell cycle of haploid *U. maydis*. During the early stages of budding, GFP-Myo5 (green) and actin (red) colocalize (**[B1]** to **[B3]**; overlay results in yellow). However, in large budded cells, actin appears at the bud neck (arrows in **[B4]** and **[B5]**), whereas most GFP-Myo5 still localizes to the growing bud tip. During cytokinesis, both GFP-Myo5 and actin concentrate at the cleavage site **(B6)**. Bar = 5 μm.

(C) Upon oxygen depletion caused by prolonged observation, GFP-Myo5 localizes to filamentous structures. The inset shows a large bud that contains filaments that are in contact with the GFP-Myo5 accumulation at the tip. Bar = 5 μm.

(D) GFP-Myo5 localization after ATP depletion. In untreated cells expressing high levels of GFP-Myo5 (FB2oGMyo5), the tip signal intensity increases **(D1)**. After treatment with CCCP, which inhibits the mitochondrial respiration chain and therefore depletes ATP, GFP-Myo5 stains long filaments **(D2)**. These structures can be disrupted by the actin inhibitor cytochalasin D (CD **[D3]**), suggesting that they are F-actin cables. Bars = 5 μm.

(E) Localization of GFP-Myo5 after the disruption of microtubules, F-actin, or inhibited myosin activity. Treatment with the solvent DMSO (not shown) or benomyl (Ben **[E1]**) at concentrations that were shown to disrupt all microtubules (20 μM) (Straube et al., 2003) does not significantly affect GFP-Myo5 distribution. However, 50 μM of the potent F-actin inhibitor latrunculin A (LatA **[E2]**) as well as 10 mM of the myosin inhibitor BDM **(E3)** abolish the polar accumulation of GFP-Myo5, suggesting that actin-dependent transport underlies the tip localization of Myo5. Bar = 5 μm.

charcoal-containing plates. Wild-type crosses led to a typical fuzzy colony appearance, which was attributable to the massive formation of dikaryotic hyphae (Figure 5, WT × WT). Δ*myo5* cells were strongly attenuated in filament formation (WT × Δmyo5), and this defect was restored in Δ*myo5* mutants expressing GFP-Myo5 (WT × Δmyo5GFPMyo5). At both permissive and restrictive temperatures, fuzzy colonies were formed in crosses of the wild type and *myo5*^{ts} (WT × Myo5^{ts}, 20 and 28°C). The formation of hyphae already was attenuated at the permissive temperature (Myo5^{ts} × Myo5^{ts}, 20°C), and no dikaryotic hyphae were seen in a cross of compatible *myo5*^{ts} at the restrictive temperature (Myo5^{ts} × Myo5^{ts}, 28°C), suggesting that Myo5 is crucial for the hyphal growth of the dikaryon. Alternatively, we considered it possible that reduced filamentation is the result of defects in the growth or formation of conjugation tubes, which precede the formation of dikaryotic hyphae. Therefore, we analyzed the role of Myo5 in mating reactions.

Mating tube formation is initiated by the perception of pheromone signals that, in addition to participating in other events, induce the *mfa* promoter. The absence of hyphae in crosses of compatible *myo5*^{ts} strains on charcoal plates at 28°C suggested that Myo5 is crucial for this initial mating reaction. Therefore, we monitored the ability to detect mating pheromone by expressing GFP under the control of the *mfa1* pro-

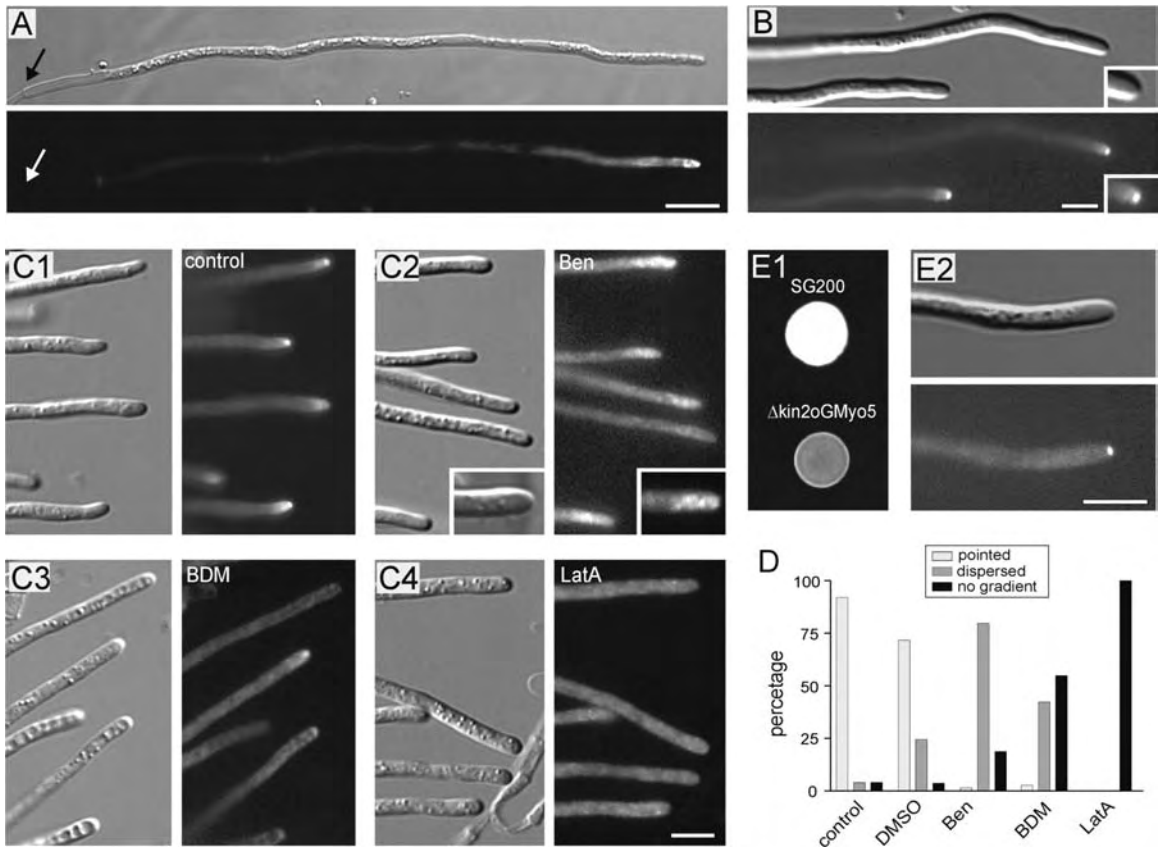

Figure 4. Localization of the GFP-Myo5 Fusion Protein in Hyphae.

(A) GFP-Myo5 localizes to the tip of dikaryotic hyphae derived from crossing FB2mGM and FB1 on charcoal plates. Note that no signal is detected at the septum (arrows) and that the tip staining varies from pointed dots to dispersed gradients (not shown). Bar = 10 μm.

(B) GFP-Myo5 in monokaryotic hyphae from liquid culture. Because of genetic manipulation, filamentous growth of strain AB33oGM can be induced by shifting cells to liquid medium containing nitrate. In these cells, GFP-Myo5 is restricted to a bright dot at the very tip of the hyphae. Note that prolonged observation results in dispersed distribution and filament staining, suggesting that these localization patterns reflect suboptimal growth conditions. Bar = 5 μm.

(C) Treatment with the solvent DMSO only slightly affects GFP-Myo5 distribution **(C1)** in AB33oGM. The addition of 20 μM benomyl (Ben) results in dispersed gradients of the fusion protein that lost the pointed localization **(C2)**. By contrast, gradients are almost absent with 10 mM BDM **(C3)** and disappear completely in the presence of 50 μM latrunculin A (LatA **[C4]**). Bar = 5 μm.

(D) Quantitative analysis of GFP-Myo5 distribution in inhibitor-treated AB33oGM hyphae.

(E) Distribution of GFP-Myo5 in hyphae lacking Kin2, a conventional kinesin from *U. maydis*. On charcoal plates **(E1)**, the control strain SG200 forms white colonies, whereas the *kin2* deletion mutant that expresses GFP-Myo5 (Δ*kin2*oGM) rarely forms filaments, thereby appearing gray on charcoal plates (Lehmler et al., 1997). In liquid culture, these hyphae contain an apical GFP-Myo5 dot **(E2)**, demonstrating that conventional kinesin is not involved in Myo5 transport to the hyphal apex. Bar = 5 μm.

moter (Spellig et al., 1996) in control and *myo5*^{ts} strains. In addition, we analyzed mating tube formation in microscopic assays that allowed the observation of tube formation caused by the confrontation of compatible partners (Snetselaar et al., 1996). The confrontation of incompatible strains neither led to GFP expression nor resulted in tube formation (Figure 6A1). By contrast, in confrontation assays of the compatible strains FB1 and FB2mG, both partners formed long conjugation tubes and GFP expression was induced in FB2mG (Figure 6A2). Similar stimulation and mating tube formation were observed in confrontations of FB1mG and FB2mG at both 20 and 28°C (Figures 6A3 and 6A4). Surprisingly, even at the permissive temperature, compatible *myo5*^{ts} strains showed neither significant GFP expression nor conjugation tube development when plated at the same distance as control cells (~200 μm; Figure 6A5). The mating reaction could be improved by a closer spacing of both partners; however, only a minor portion of the cells were stimulated and produced short mating projections (Figure 6A6). These tubes were not formed under restrictive conditions (Figure 6A7). Interestingly, *myo5*^{ts} cells were able to stimulate control cells and mating tube formation in FB1mG (Figure 6A8), suggesting that pheromone secretion is not impaired in these myosin mutants.

The observed defect of *myo5*^{ts} mutants in signal perception and tube formation was confirmed using synthetic pheromone in liquid culture (a kind gift of M. Tönnis and H. Kessler), which induces the mating reaction and conjugation tube formation (Spellig et al., 1994). After 8 h at 20°C, most cells of the control strain FB2mG reacted to the pheromone by tube formation (Figure 6B1; GFP signal in 82.2 ± 7.3% of all cells, with 140 cells in two experiments), and this always coincided with GFP expression (Figures 6B1 and 6B2). By contrast, in the same conditions, less than one-third of *myo5*^{ts} mutant cells were stimulated (Figure 6C1; GFP signal in 28.6 ± 7.6% of all cells, with 180 cells in two experiments) and no conjugation hyphae were formed. Exposure to pheromone for an additional 6 h did not increase *mfa*-induced GFP expression but led to short tube-like extensions (Figure 6C2; 14 h at 20°C) that showed the same length as the filaments observed in confrontation assays (Figure 6A6; total cell length on plates: 43.9 ± 8.0 [n = 13], cell length in liquid: 47.7 ± 5.8 [P: 0.3004; not significant at α0.05]). In summary, our data demonstrate a crucial requirement for Myo5 in conjugation tube formation. Surprisingly, tube formation and signal perception in *myo5*^{ts} mutants already was impaired at the permissive temperature, which emphasizes the importance of Myo5 in the mating of *U. maydis*.

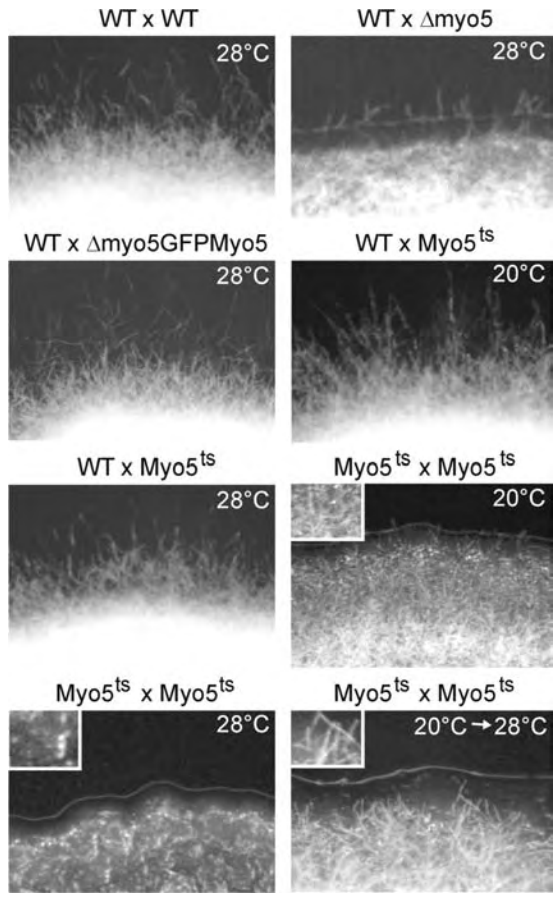

Figure 5. Analysis of the Formation of Dikaryotic *myo5*^{ts} Hyphae on Charcoal-Containing Plates.

Wild-type strains (WT × WT, 28°C) formed white colonies that consist mainly of dikaryotic hyphae. Crossing of wild-type and Δ*myo5* strains shows drastically impaired filament formation (WT × Δmyo5, 28°C) that is restored by expression of the functional GFP-Myo5 fusion protein (WT × Δmyo5GFPMyo5). Mating reactions of wild-type and temperature-sensitive *myo5*^{ts} strains show no defects in filament formation at permissive and restrictive temperatures (WT × Myo5^{ts}, 20 and 28°C). The formation of dikaryotic hyphae is impaired in crosses of *myo5*^{ts} cells under permissive conditions (Myo5^{ts} × Myo5^{ts}, 20°C) and is abolished completely at the restrictive temperature (Myo5^{ts} × Myo5^{ts}, 28°C). However, filamentation is restored by incubation at the permissive temperature for 2 days followed by growth at the restrictive temperature (Myo5^{ts} × Myo5^{ts}, 20 to 28°C). This finding suggests that *myo5*^{ts} strains fail to form filaments at an early stage of the mating process but hyphae appear after the initial fusion is complete.

Myo5 Is Required for the Formation and Proper Morphology of Dikaryotic Hyphae

To circumvent the observed mating defects of *myo5*^{ts} strains, we incubated crosses of compatible *myo5*^{ts} strains for 2 days at the permissive temperature and shifted them to restrictive conditions for an additional 12 h. As expected, this treatment allowed hyphae formation (Figure 5; Myo5^{ts} × Myo5^{ts}, 20 to 28°C). To ascertain that these filaments were products of cell fusion, we expressed yellow-shifted fluorescent protein (YFP) in one strain and cyan-shifted fluorescent protein (CFP) in the compatible partner (Figure 7A). Wild-type hyphae at 20°C (Figure 7B) and *myo5*^{ts} mutant hyphae at 20°C (Figure 7C) contained both colors, confirming that they derived from cell fusion of compatible strains. *myo5*^{ts} sporidia showed severe defects at 34°C within 2 to 6 h, indicating that the mutant protein is inactive (Figure 2F3). Consequently, we shifted *myo5*^{ts} hyphae to 34°C for an additional 12 h and obtained mutant hyphae that were much thicker than control hyphae and grew highly irregularly (Figure 7D), with strong chitin distribution along the length of the

hyphae (Figure 7E). A similar growth phenotype was observed at 28°C, suggesting that this temperature already is sufficient to inactivate Myo5^{ts} (Figure 7F). These data indicate that Myo5 is not required for the polar growth of dikaryotic infection hyphae but that its activity is crucial for proper hyphal morphogenesis.

The Reduced Pathogenicity of *myo5^{ts}* Mutants Is Attributable to Defects in Mating and Early Infection in Planta

To investigate the relevance of the observed defects of *myo5^{ts}* mutants for virulence, we infected maize plants and incubated them in a phytochamber for up 13 to 17 days under permissive or restrictive conditions. In control experiments, wild-type hyphae induced anthocyan production in all plants and induced tumors in >80% of plants at permissive and restrictive temperatures (Table 2). By contrast, even at the permissive temperature, *myo5^{ts}* strains showed drastically reduced virulence after 17 days, and even after 24 days, no further tumor formation was observed, suggesting that *myo5* mutants are unable to infect plants. Under restrictive conditions, no symptoms were observed (Table 2). Infection of young maize plants with the fluorescent control strains FB1Y and FB2C led to a network of filaments on the plant epidermis that could be stained with Cal-

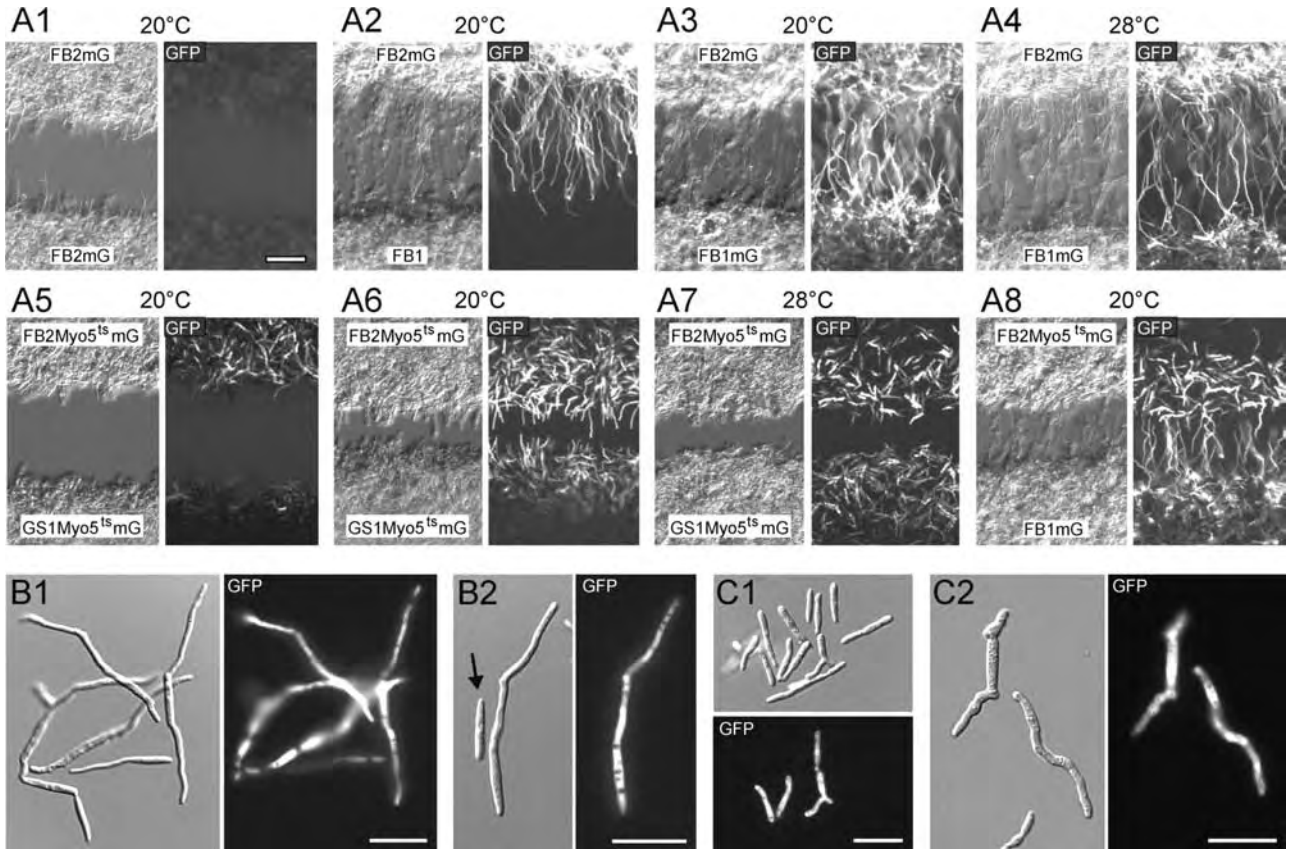

Figure 6. Defects of *myo5^{ts}* Mutants during Early Steps of Mating.

(A) At the beginning of mating and before conjugation tube formation, secreted pheromone of the opposing mating partner is recognized and *mfa1* expression increases. In *myo5^{ts}* and control strains, GFP was put under the control of the *mfa1* promoter, which allows the visualization of pheromone perception. In addition, the ability to form conjugation tubes was monitored in confrontation assays, in which adjacent mating partners bridge large distances by the formation of conjugation hyphae. In a negative control of cells of the same mating type, tubes are not formed and *mfa*-GFP expression is not detected **(A1)**. In compatible confrontations of compatible strains, long conjugation tubes are formed, but only the *mfa*-GFP–containing strain shows GFP fluorescence **(A2)**, whereas both the perception of pheromone and tube formation are detectable in confrontation assays of FB2mG and FB1mG at 20°C **(A3)** and 28°C **(A4)**. By contrast, plating *mfa*-GFP–containing *myo5^{ts}* strains at the permissive temperature does not result in tube formation, nor are cells properly stimulated **(A5)**. The mating reaction is improved after reducing the distance between the compatible *myo5^{ts}* strains, but only short hyphae are formed **(A6)**. Filamentation of mutant cells is abolished at 28°C **(A7)**. However, *myo5^{ts}* mutants are able to stimulate compatible control cells **(A8)**. All images were taken after 14 h of incubation. Bar in **(A1)** = 50 μm.

(B) Treatment of strain FB2mG with synthetic *a1*-mating pheromone for 8 h at 20°C induces the expression of *mfa*-GFP and the formation of hyphal extensions that most likely resemble conjugation tubes **(B1)**. Occasionally, cells without GFP expression are observed that also do not grow filamentously **(B2)**. Bars = 20 μm.

(C) FB2Myo5^{ts} mG cells treated with pheromone are only partially stimulated and do not form any tubes after 8 h at 20°C **(C1)**. After 14 h, only stimulated cells, identified by their GFP signals, form short and irregular extensions that resemble those depicted in **(A6)**. Bars = 20 μm.

cofluor (Figure 8A1). Detection of both CFP and YFP in the same cell confirmed that these hyphae derived from fusion of the compatible strains (Figure 8A2; the arrow points to stomata). By contrast, the compatible strains FB2Myo5^{ts} and GS1Myo5^{ts} almost never fused, and even closely adjacent cells remained separated, as confirmed by CFP/YFP detection (Figure 8B1). Only occasionally was cell fusion observed (Figure 8B2), which gave rise to long dikaryotic infection hyphae (Figure 8B3).

Interestingly, *myo5^{ts}* mutants triggered anthocyan production in ~20% of all plants, which is indicative of the penetration of plant tissue (Banuett and Herskowitz, 1996), but they failed to induce tumors. This finding suggested that a significant portion of the observed mutant hyphae entered the plant but did not complete their pathogenic development. To analyze this phenomenon, we used a Chlorazole black E–based staining method (Brundett et al., 1996; Brachmann et al., 2003) that enabled us to perform a three-dimensional analysis of wild-type and *myo5^{ts}* hyphae in early infection stages of cleared plant tissue. One day after infection, wild-type cells already penetrated the epidermis (Figure 9A, top view of infection site; the arrowhead marks the entry site) and invaded the underlying mesophyll (Figure 9A; see also supplemental data online). By contrast, infection of *myo5^{ts}* took much longer, and infection sites were found only rarely at 6 days after infection (Figure 9B). *myo5^{ts}* hyphae invaded the plant (Figure 9B, the entry site is marked by the arrowhead) but formed numerous and swollen branches within the plant mesophyll (Figure 9B; see also supplemental data online). A direct comparison of wild-type and *myo5^{ts}* structures in planta demonstrated the extent of branching and swelling found in *myo5* mutants (Figure 9C; *Z*-axis projection of all planes in planta). Later infection stages were never observed, indicating that *myo5^{ts}* hyphae were unable to complete their pathogenic program, most likely because Myo5 is crucial for further invasive growth within its host plant. Such additional roles of Myo5 in planta might be similar to those found in sporidia and dikaryotic hyphae, because GFP-Myo5 localized to growing tips and septa of hypha in planta (Figures 9D1 to 9D3). Furthermore, GFP-Myo5 was found in early and late spores (Figures 9D4 and 9D5), indicating that Myo5 also supports spore formation.

Table 2. Pathogenicity of Myo5^{ts} Mutants and Wild-Type Strains

	20°C[a]			28°C[b]		
Strain	Anthocyanin	Tumor	No.	Anthocyanin	Tumor	No.
Wild type	100%	96.9%	(32)	100%	82%	(39)
Myo5^{ts}	19.4%	2.7%	(36)	0%	0%	(36)

All values are given as percentage of plants with anthocyanin symptoms or tumors. The number of plants analyzed is indicated in parentheses.
[a] Plants harvested at 17 days after infection.
[b] Plants harvested at 13 days after infection.

DISCUSSION

The pathogenic development of *U. maydis* begins when compatible haploid sporidia recognize the opposite mating partner. After transcriptional activation of mating-specific genes, including the induction of *mfa1* expression (Urban et al., 1996), both mating partners undergo a morphological transition from budding yeast to a tip-growing filament. These conjugation tubes are characterized by directed growth toward the pheromone source (Spellig et al., 1994). After fusion of the mating partners, a dikaryotic infection hypha is formed that contains two nuclei and the cytoplasm of both mating partners. This hypha continues polar tip growth to find the invasion site, where it forms an appressorium-like structure that penetrates the plant epidermis (Banuett and Herskowitz, 1996). Therefore, morphological transitions are closely linked to the virulence of *U. maydis*. However, the mechanisms that govern these transitions are poorly understood.

Myo5, a Class-V Myosin Required for Morphogenesis and Cytokinesis in Yeast-Like Sporidia

Based on sequence similarity and the predicted domain structure, Myo5 is most likely a class-V myosin in *U. maydis*. The genomic sequence of *U. maydis* that was published recently (for URL, see Methods) contains two additional myosins belonging to class I and class II and one myosin-chitin synthase (data not shown) but no other class-V myosin. Therefore, the myosin gene family in *U. maydis* is more closely related to that of filamentous fungi (for overview, see Mulvihill and Hyams, 2003) than to that of the unicellular fungi *S. cerevisiae* and *S. pombe*, both of which have two class-V myosins (Johnston et al., 1991; Haarer et al., 1994; Motegi et al., 2001; Win et al., 2001) but do not contain a myosin-chitin synthase. This finding is interesting, because *U. maydis* also grows like unicellular yeast, suggesting that this similarity in myosin motors to filamentous fungi is attributable to the ability of *U. maydis* to form hyphae. However, the defect in polar growth and cytokinesis of *myo5* mutant sporidia is reminiscent of *myo52^{+}/myo4^{+}* mutants in *S. pombe* (Motegi et al., 2001; Win et al., 2001), suggesting that in this yeast-like growth stage myosin functions are conserved between fission yeast and *U. maydis*. Further studies of myosins in *U. maydis* are required to elucidate the importance of these motors in the yeast-like and hyphal growth of this dimorphic fungus.

A functional interaction of Myo5 and F-actin is indicated by the tight binding of GFP-Myo5 to cytochalasin-sensitive filaments in the absence of ATP and by the motility of GFP-Myo5 under certain stress conditions. Myo2p, a class-V myosin in *S. cerevisiae*, is the main organelle transporter in this yeast, and it is implicated in secretory vesicle transport, polar growth, and vacuole inheritance (Johnston et al., 1991; Govindan et al., 1995; Hill et al., 1996). In *S. pombe*, two class-V myosins participate in the delivery of secretory vesicles and in cytokinesis (Motegi et al., 2001; Win et al., 2001), indicating that class-V myosins are organelle transporters in fungi. This is consistent with the findings of studies in higher eukaryotes, in which class-V myosins govern the transport of membranous organelles, including endoplasmic reticulum vesicle and Golgi-derived secretory vesicles (for reviews, see Reck-Peterson et al., 2000; Langford, 2002).

The observed defects in Δ*myo5* cells in morphogenesis and cytokinesis are most consistent with such a role of this myosin motor in vesicle transport and polar exocytosis during tip growth and cell separation in *U. maydis*. However, defects in endocytosis result in similar morphogenic defects in *U. maydis* (Wedlich-Söldner et al., 2000), raising the possibility that Myo5 is involved in endocytosis rather than secretion. Experiments using the endocytic marker FM4-64 revealed that endocytic uptake occurs at the whole cell surface (Wedlich-Söldner et al., 2000), although Myo5 is concentrated mainly at the growing tip of the cell. Moreover, Myo5^{ts} mutant cells are impaired neither in the uptake of the endocytic marker dye FM4-64 nor in the delivery of the dye to the vacuole (data not shown). Therefore, we consider it unlikely that Myo5 participates in the endocytosis of *U. maydis*. At present, the actual cargo of Myo5 is unknown. Evidence exists that Myo2p transports chitin synthase in *S. cerevisiae* (Santos and Snyder, 1997). In *U. maydis myo5* null mutants, chitin and chitin synthase distribution is unaltered, indicating that Myo5 is not involved in the delivery of chitin synthases. However, *U. maydis* contains eight different chitin synthases (I. Weber and G. Steinberg, unpublished data), and the antibody might recognize only a subset of these enzymes. Al-

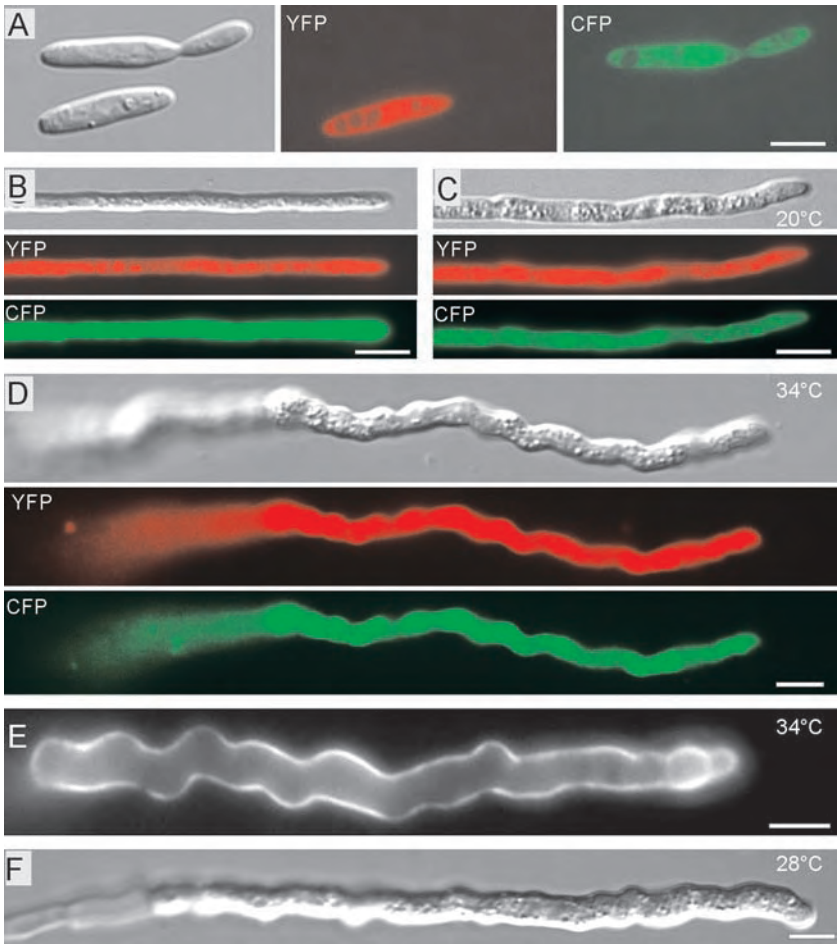

Figure 7. Analysis of the Role of Myo5 in Dikaryotic Hyphae.

(A) Expression of yellow- and cyan-shifted derivatives of GFP (YFP and CFP) allows the identification of mating partners that contain compatible mating loci. Signals are given in false colors. Bar = 5 μm.

(B) Fusion of compatible haploid wild-type strains expressing either YFP or CFP results in dikaryotic hyphae that contain both fusion proteins (YFP in red; CFP in green). Bar = 5 μm.

(C) Crossing CFP and YFP expressing compatible *myo5^{ts}* strains at the permissive temperature resulted in straight but slightly thicker dikaryotic hyphae, as confirmed by the detection of both YFP (red) and CFP (green) in a single cell. Bar = 5 μm.

(D) After mating at the permissive temperature and growth for another day at the restrictive temperature, dikaryotic mutant hyphae are thicker and grow irregularly. Note that this image is given at a lower magnification than that in **(C)**. Bar = 5 μm.

(E) Chitin staining in *myo5^{ts}* hyphae under restrictive conditions. In contrast to wild-type hyphae, which accumulate chitin at the growing hyphal tip (not shown), WGA staining reveals the irregular composition of the mutant cell wall. This finding suggests that the abnormal morphology of *myo5^{ts}* hyphae is attributable to defects in the cell wall. Bar = 5 μm.

(F) At 28°C, *myo5^{ts}* hyphae show the temperature-dependent phenotype. Bar = 5 μm.

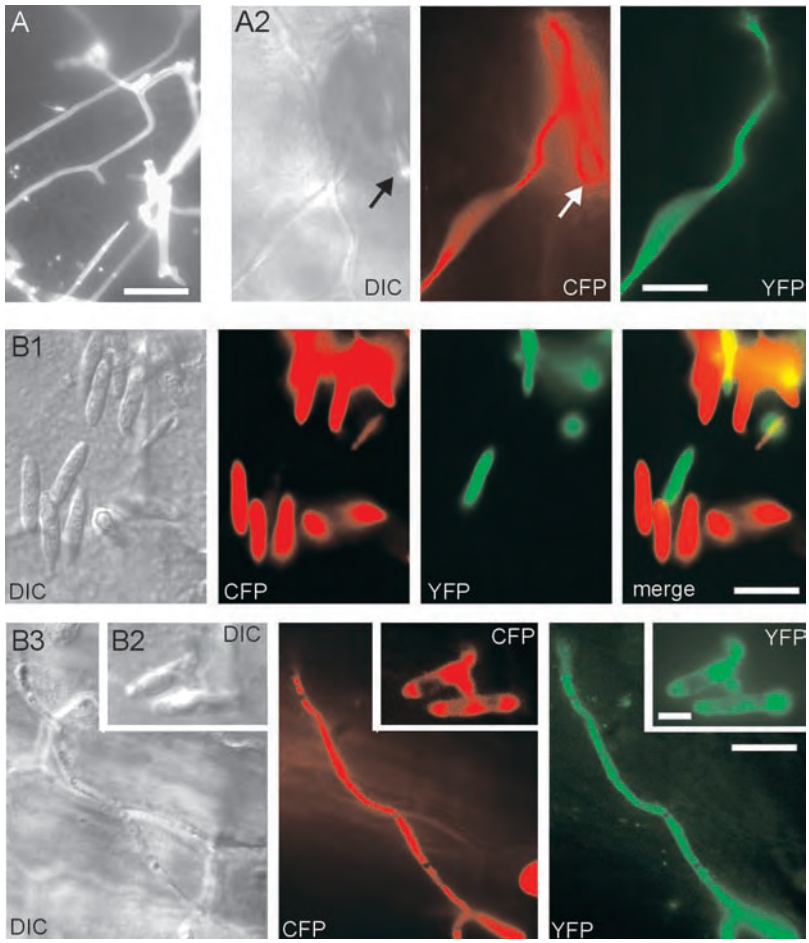

Figure 8. *Myo5*^{ts} Mutants Cells on the Epidermis of the Host Plant.

(A) Infections of young maize plants with a mixture of compatible wild-type cells results in a network of hyphae that can be detected on the plant surface after 2 days by Calcofluor staining of the fungal cell wall **(A1)**. These filaments are derived from the fusion of mating partners, as confirmed by infection with CFP- and YFP-expressing compatible strains **(A2)**. DIC, differential interference contrast. Bars = 10 μm.

(B) Infection of plants at 20°C with compatible *myo5*^{ts} strains that express YFP or CFP demonstrates that most mutant cells do not fuse with adjacent mating partners, and only rarely do two cells fuse, thereby expressing both CFP and YFP **(B2)**. Consistent with the in vitro observation on charcoal plates, the fusion of compatible cells results in the formation of long dikaryotic infection hyphae **(B3)**. Bars = 10 μm in **(B1)** and **(B3)** and 5 μm in **(B2)**.

ternatively, Myo5 could transport other wall enzymes, such as α-glucan, which is a cargo of Myo52 in *S. pombe* (Win et al., 2001).

myo5^{ts} Mutants Show Impaired Pheromone Perception and Conjugation Tube Formation

The initial step of pathogenic development in *U. maydis* is the perception of the mating pheromone of the opposite partner. This is followed by the upregulation of several genes, including *mfa1* (Urban et al., 1996), which encodes the *a1* mating pheromone precursor. We made use of a construct containing the promoter of *mfa1* fused to GFP, which allows the visualization of pheromone-dependent stimulation of the cell during mating (Spellig et al., 1996). In control experiments, the presence of a mating partner activated the *mfa* promoter and induced GFP expression, and the same reaction was found after the stimulation of FB2mG with synthetic pheromone in liquid cultures, with >85% expressing GFP, which always coincided with tube formation. By contrast, Δ*myo5* mutants never formed mating tubes (data not shown), and *myo5*^{ts} mutants were much less sensitive to mating pheromone on plates and in liquid culture even at the permissive temperature. Even after extended periods in synthetic *a1* pheromone, most cells neither showed GFP expression nor formed a conjugation tube. Furthermore, the few mating projections found remained short and much thicker than those of control cells.

This result is most surprising, because the *myo5*^{ts} allele facilitates almost normal yeast-like and hyphal growth at 20°C. Therefore, we consider it likely that Myo5 is particularly important during the mating reaction. In *S. cerevisiae*, the pheromone-induced clustering of receptors depends on intact

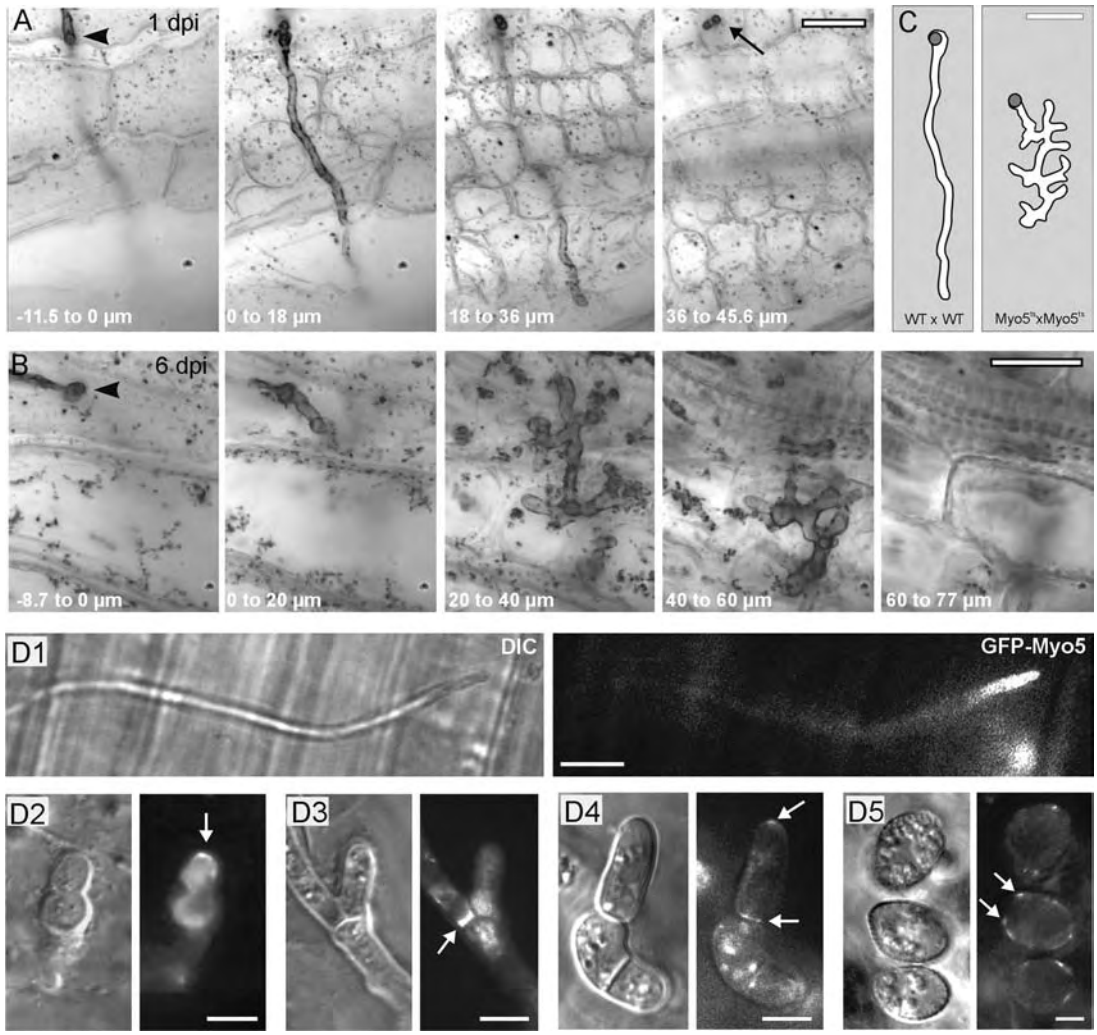

Figure 9. Penetration of the Host Plant by Wild-Type and *myo5*^{ts} Hyphae.

(A) Series of minimal *Z*-axis projections showing a top view of the initial infection state of wild-type hypha at 20°C. One day after infection (1 dpi), wild-type hyphae form appressoria on the plant surface (arrowhead; −11.5 to 0 μm), usually invade the plant as an unbranched hypha (0 to 18 μm), and reach through the epidermis into the underlying mesophyll of the leaf (18 to 36 μm). Note that hyphae often penetrate into much deeper regions of the leaf (the arrow points to a branch that leaves the focal plane). Bar = 10 μm.

(B) *myo5*^{ts} mutant hypha 6 days after infection (6 dpi) at 20°C. An appressorium is formed (arrow; 8.7 to 0 μm), and the hypha penetrates straight through the epidermis (0 to 20 μm), but it does form multiple and swollen branches within the leaf mesophyll (40 to 60 μm and 60 to 77 μm). Note that images are top views of minimal *Z*-axis projections of planes within the indicated range. Bar = 10 μm.

(C) Graph based on minimum projections of 456 planes (WT × WT) and 771 planes (Myo5^{ts} × Myo5^{ts}) that illustrates the dimensions and extent of branching of *myo5*^{ts} hyphae. The gray circle indicates the site of entry into the plant. Bar = 10 μm.

(D) GFP-Myo5 localization in planta. GFP-Myo5 localizes in tips of growing hyphae on the plant surface **(D1)**. Six days after infection, hyphae differentiate inside infected plants and GFP-Myo5 concentrates at the tips of lobed branches **(D2)** and septa **(D3)**. After 13 to 14 days, hyphal fragmentation occurs, cells become rounded, and GFP-Myo5 appears at the tips and septa of these cells (arrows in **[D4]**). Finally, spore maturation occurs and spore walls are formed. GFP-Myo5 localizes in patches at the cell periphery. DIC, differential interference contrast. Bars = 5 μm.

F-actin (Ayscough and Drubin, 1998), and it is tempting to speculate that Myo5 is involved in the F-actin transport of pheromone receptors in *U. maydis*. In *myo5*^{ts} cells, such a process might be impaired, which could explain why *myo5* mutants show reduced sensitivity to mating pheromones. However, at present, we have no further evidence for such a model. A mating-specific role for Myo5 would be consistent with the existence of a class-V myosin in the mating loci of the pathogenic basidiomycete *Cryptococcus neoformans* (Karos et al., 2000; Lengeler et al., 2002). The tail of Myo5 shares 47% sequence identity with this motor (compared with 31% with the tail of *S. cerevisiae* Myo2p and 17% with the tail of Myo52/Myo4 of *S.*

pombe), suggesting that both myosins have similar cellular functions in mating and pathogenic development in the pathogens *U. maydis* and *C. neoformans*. However, a particular role for the *C. neoformans* class-V myosin in mating has not been described. In summary, our data demonstrate the particular importance of Myo5 in pheromone-based signaling as well as mating tube formation. Further studies are under way to elucidate the molecular details of the mechanism underlying these fascinating observations.

The Morphology of Dikaryotic Hyphae Depends on Myo5

The *myo5^{ts}* cells were completely unable to form dikaryotic hyphae on charcoal plates, most likely as a result of the described mating defect. To circumvent this problem, we incubated mutant strains at 20°C, which allowed mating reactions and cell fusion, and shifted these preexisting hyphae to restrictive conditions. Although Myo5 is essential for conjugation tube formation, it is dispensable for the growth and cell polarity of dikaryotic hyphae. Mutant hyphae remained unbranched and still grew in a polar manner, suggesting that basic cell polarity is governed by other mechanisms. It was shown that the microtubule-based traffic of endosomes is important for hyphal morphogenesis in *U. maydis* (Wedlich-Söldner et al., 2000), suggesting that both F-actin and microtubules participate in the hyphal tip growth of *U. maydis*. Much evidence exists for a crucial role of F-actin in fungal tip growth (summarized by Heath, 1995). On the other hand, microtubules are involved in the apical organization of the Spitzenkörper, which is a specialized vesicle accumulation implicated in the polar exocytosis of fungal hyphae (Riquelme et al., 1998). Both kinesin and dynein motors are thought to participate in organizing the Spitzenkörper (Seiler et al., 1997; Riquelme et al., 2000). The biologically active fusion protein GFP-Myo5 resides in a dot at the apex of growing hyphae, suggesting that Myo5 could deliver secretory vesicles to the Spitzenkörper or could participate in the organization of this remarkable organelle. However, the precise role of Myo5 in apical tip growth remains to be determined and may require ultrastructural analysis of Myo5 distribution or the identification of the Myo5 cargo.

Myo5 Is Essential for the Pathogenicity of *U. maydis*

Because mating is an indispensable requirement for the infection of plants, it was not surprising that *myo5^{ts}* mutants showed drastically reduced virulence. However, some dikaryotic hyphae were formed that occasionally penetrated the plant epidermis by forming appressoria and direct invasive growth. Surprisingly, mutant hyphae did not continue their infection but started extensive branching within the mesophyll of the infected leaf. This is even more astonishing because this phenotype occurred at the permissive temperature, at which most morphogenic defects of haploid sporidia were restored. Therefore, we consider it possible that Myo5 is of central importance during the invasive growth of *U. maydis* and that minor defects of the *myo5^{ts}* allele at the permissive temperature become crucial during hyphal growth in the plant. In addition, the infection process of *myo5^{ts}* mutants was slowed considerably compared with that in the wild type, raising the possibility that this changes the conditions for infection. The mechanisms of the temporal regulation of pathogenic development in *U. maydis* are not known, but we consider it likely that the physiological state of the host cell and the fungus influences fungal virulence. In other words, 6 days after infection might simply be too late for a successful infection of *myo5^{ts}* hyphae. At present, we cannot distinguish between these possibilities. However, Myo5 clearly is of central importance for the pathogenic development of *U. maydis*, and the observed phenotypes and the localization of Myo5-GFP in early and late spores suggest multiple roles of this motor during infection of the host plant.

METHODS

Identification and Cloning of *myo5* and *myo1*

The gene *myo5* was identified in a PCR-based approach using *Ustilago maydis* genomic DNA and degenerate primers based on conserved regions (MyoV1, 5′-TTYWAYGAYAAYCARCC-3′; and MyoV4, 5′-GCICKRAARAADATYTTNG-3′). PCR was performed in 30 cycles (94°C for 1 min, a gradient from 45 to 56°C over 1.5 min, and 72°C for 1 min) in a Robocycler (Stratagene). The obtained amplicon was used to screen a cosmid library (Bölker et al., 1995), and the complete *myo5* gene was cloned. Double-stranded sequencing followed standard procedures.

Strains, Plasmids, and Growth Conditions

Strains FB1 (*a1b1*) and FB2 (*a2b2*) have been described (Banuett and Herskowitz, 1989) (for details of plasmids and strains, see Table 1). Deletion of *myo5* was performed by homologous replacement of nucleotides −134 to +2581 with a hygromycin resistance cassette, resulting in strain FB2ΔMyo5. The temperature-sensitive (*ts*) strain FB2Myo5^{ts} was generated by insertion of pMyo5^{ts} that contained the full-length *myo5* gene with a point mutation (E534K) that confers temperature sensitivity to Myo2p in *Saccharomyces cerevisiae* (Lillie and Brown, 1994) in the succinate dehydrogenase locus of FB2ΔMyo5. The compatible strain GS1Myo5^{ts} was generated by segregation analysis of teliospores after plant infection with FB1 and FB2Myo5^{ts}. For localization, the GFP plasmids pMGmyo5 and pOGmyo5C or pOGmyo5H, containing *gfp-myo5* under the control of the native *myo5* promoter or the constitutive *otef* promoter (Spellig et al., 1996), respectively, were introduced ectopically into strains FB2ΔMyo5 and AB33 (Brachmann et al., 2001), resulting in the strains FB2mGM, FB2oGM, and AB33oGM. The kinesin-deficient strain SG200Δ*kin2* was generated by replacing *kin2* in the solopathogenic strain SG200 that is a derivative of SG100 (Bölker et al., 1995) and that occasionally forms hyphae in liquid culture. In this strain, pOGmyo5H was integrated ectopically to obtain SG200ΔKin2oGM.

Pheromone stimulation was monitored by the integration of pmfa1GFP, which contained GFP under the control of the *mfa1* promoter that is activated upon pheromone recognition (Spellig et al., 1996) in strains FB1, FB2, FB2Myo5^{ts}, and GS1Myo5^{ts}, resulting in FB1mG, FB2mG, FB2Myo5^{ts}mG, and GS1Myo5^{ts}mG. Cell fusion after mating reactions was confirmed by crossing FB1Y or GS1Myo5^{ts}Y, which contained the yellow-shifted fluorescent protein (YFP; Clontech, Palo Alto, CA) under the control of the *otef* promoter, with FB2C or FB2Myo5^{ts}C, which expressed the cyan-shifted fluorescent protein (CFP; Clontech). Strains were grown at 28°C in complete medium (CM) (Holliday, 1974). Solid medium contained 2% (w/v) bacto-agar. Conditional temperature-sensitive strains were placed in water baths at 20°C for permissive growth and at either 28 or 34°C for restrictive growth. Strains were crossed on char-

coal-containing plates (Holliday, 1974) and observed after 2 days. To obtain dikaryotic *myo5*^{ts} hyphae, the compatible strains FB2Myo5^{ts} and GS1Myo5^{ts} were mixed and incubated on charcoal plates for 2 days before being kept at 28°C overnight. Confrontation assays were performed as described (Snetselaar et al., 1996) and analyzed after 14 to 15 h. Plant infections were performed as described (Gillissen et al., 1992). The filamentous growth of AB33oGM was induced by shifting cells that were grown in CM-glucose to nitrate minimal medium-glucose (Holliday, 1974). Cells were analyzed after 8 to 12 h of growth in NM-glucose at 28°C.

Sequence Analysis

Alignments were made with CLUSTAL X (Thompson et al., 1997). Phylogenetic dendrograms were constructed using MEGA 2.1 (Kumar et al., 2001; www.megasoftware.net), with the minimum evolution or maximum parsimony algorithm and gap deletion option. Domain analysis was performed using Pfam and Paircoil (www.expasy.ch). PEST sites were predicted by PESTfind (embl.bcc.univie.ac.at/htbin/embnet/PESTfind). The sequence of a class-I myosin, UmMyo1, was obtained by PCR (described elsewhere), and the sequence of a class-II myosin, UmMyo2, was obtained from the genome sequence of *U. maydis* published recently by the Whitehead Institute (http://www-genome.wi.mit.edu/annotation/fungi/ustilago_maydis/). Both were included in the dendrogram.

Immunofluorescence Wheat Germ Agglutinin Staining and Microscopy

Immunofluorescence procedures followed published protocols (Straube et al., 2003). Monoclonal anti-actin antibody (1:100, clone JLA20; Oncogene, Darmstadt, Germany), anti-α-tubulin (1:200; Oncogene), and chitin synthase polyclonal antibody (1:200; Sietsma et al., 1996) were diluted in PBS and 0.1% milk powder. Secondary antibodies (Jackson, West Grove, PA) were used at 1:200. Wheat germ agglutinin staining was performed as described previously (Wedlich-Söldner et al., 2000). Light microscopy used a Zeiss Axiophot (Jena, Germany), and standard fluorescein isothiocyanate, 4′,6-diamidino-2-phenylindole, and rhodamine filter sets were used for epifluorescence. For colocalization studies, YFP and CFP were analyzed with specific filter sets (YFP, BP500/20, FT515, and BP535/30; CFP, BP436, FT455, and BP480-500). *Z*-axis imaging stacks were generated by acquiring images with 100-nm step intervals using a CoolSNAP-HQ charge-coupled device camera (Photometrics, Tucson, AZ) and a PiEFOC Piezo electric fast-focus device (Physik Instrumente, Waldbronn, Germany), both controlled by the imaging software MetaMorph (Universal Imaging, West Chester, PA).

Image Processing and Quantitative Analysis

Digital images or sequences were captured with a cooled charge-coupled device camera (4742-95 [Hamamatsu] or CoolSNAP-HQ). Image two-dimensional deconvolution and *Z*-projections were performed with MetaMorph. Measurements and image processing, including adjustment of brightness, contrast, and γ-values, were performed with ImageProPlus (Media Cybernetics, Gleichen, Germany), MetaMorph (Universal Imaging), and Photoshop (Adobe, Mountain View, CA). Statistical analysis by two-tailed *t* test at $\alpha = 0.05$ was performed using Prism (GraphPad Software, San Diego, CA). All values are given as means ± SD unless stated otherwise.

Live Cell Observation, Inhibitor Studies, and Pheromone Stimulation Experiments

For observation of cells from liquid culture, logarithmically growing cells were embedded in 1% low-melting-point agarose and mounted on slides. Microscopic preparations were observed no longer than 10 min to prevent defects caused by oxygen depletion. Because of the sensitivity of the tip staining of GFP-Myo5, cells were taken freshly from shaking cultures and observed immediately without any mounting. Where necessary, anoxia could be induced by long-term incubation of cells under the cover slip (>15 min). For all inhibitor experiments, 500 μL of cell suspension was incubated in a 2-mL reaction tube and either Benomyl at 20 μM (10 mM in DMSO; Fluka, Milwaukee, WI), latrunculin A at 50 μM (20 mM in DMSO; kindly provided by Karen Tenney, University of California, Santa Cruz), 2,3-butanedione monoxime at 10 mM (500 mM in water; Sigma), or carbonyl cyanide *m*-chlorophenylhydrazone at 100 μM (10 mM in DMSO; Sigma) was added. In control experiments, the corresponding amount of the solvent DMSO was used. Reaction tubes were incubated at room temperature for 30 to 60 min with gentle shaking. For pheromone response studies, synthetic pheromone at 1 μg/mL (a kind gift of M. Tönnis and H. Kessler; 1 mg/mL stock in DMSO) was added to 500 μL of cell suspension in a 2-mL reaction tube and incubated at 20°C at 200 rpm for 8 or 14 h, followed by microscopic analysis.

Observation of Live Cells on Leaves and Fixed Fungal Hyphae in Plant Tissue

Infection of plant leaves was analyzed on the third outer leaf ~1 cm below the infection site. For in vivo observation, the lower epidermis and most of the leaf mesophyll was removed to reduce nonspecific autofluorscence of chloroplasts. Cells and hyphae attached to the upper epidermis were observed directly in epifluorescence using specific YFP and CFP filter sets (see above). For Calcofluor staining, leaves were incubated for 1 min in 100 μg/mL Calcofluor in water, rinsed thoroughly, and analyzed immediately. For the detection of early infection stages inside plant tissue, Chlorazole black E staining was performed as described previously (Brachmann et al., 2003).

Upon request, materials integral to the findings presented in this publication will be made available in a timely manner to all investigators on similar terms for noncommercial research purposes. To obtain materials, please contact Gero Steinberg, gero.steinberg@staff.uni-marburg.de.

Accession Number

The accession number for *myo5* is AJ577236.

ACKNOWLEDGMENTS

The authors thank M. Tönnis and H. Kessler for synthetic pheromone, D. Assmann for technical support, and F. Feldbrügge for discussion. We are grateful to R. Kahmann for much support and helpful advice. H. Sietsma and H. Deising are acknowledged for providing antibodies. This work was supported by a grant from the Deutsche Forschungsgemeinschaft (SFB 413, SP 1111).

Received August 9, 2003; accepted September 29, 2003.

REFERENCES

Ayscough, K.R., and Drubin, D.G. (1998). A role for the yeast actin cytoskeleton in pheromone receptor clustering and signalling. Curr. Biol. **8,** 927–930.

Azarkina, N., and Konstantinov, A.A. (2002). Stimulation of menaquinone-dependent electron transfer in the respiratory chain of *Bacillus subtilis* by membrane energization. J. Bacteriol. **184,** 5339–5347.

Banuett, F. (1995). Genetics of *Ustilago maydis*, a fungal pathogen that induces tumors in maize. Annu. Rev. Genet. **29,** 179–208.

Banuett, F., and Herskowitz, I. (1989). Different a alleles of *Ustilago maydis* are necessary for maintenance of filamentous growth but not for meiosis. Proc. Natl. Acad. Sci. USA **86,** 5878–5882.

Banuett, F., and Herskowitz, I. (1996). Discrete developmental stages during teliospore formation in the corn smut fungus, *Ustilago maydis*. Development **122,** 2965–2976.

Banuett, F., and Herskowitz, I. (2002). Bud morphogenesis and the actin and microtubule cytoskeletons during budding in the corn smut fungus, *Ustilago maydis*. Fungal Genet. Biol. **37,** 149–170.

Bölker, M., Genin, S., Lehmler, C., and Kahmann, R. (1995). Genetic regulation of mating and dimorphism in *Ustilago maydis*. Can. J. Bot. **73,** 320–325.

Bölker, M., Urban, M., and Kahmann, R. (1992). The a mating type locus of *U. maydis* specifies cell signaling components. Cell **68,** 441–450.

Brachmann, A., Schirawski, J., Müller, P., and Kahmann, R. (2003). An unusual MAP kinase is required for efficient penetration of the plant surface by *Ustilago maydis*. EMBO J. **22,** 2199–2210.

Brachmann, A., Weinzierl, G., Kamper, J., and Kahmann, R. (2001). Identification of genes in the bW/bE regulatory cascade in *Ustilago maydis*. Mol. Microbiol. **42,** 1047–1063.

Brundett, M., Bougher, N., Dell, B., Grove, T., and Malajcuk, N. (1996). Working with Mycorrhizas in Forestry and Agiculture, Monograph 32. (Canberra, Australia: Australian Centro for International Agricultural Research).

Catlett, N.L., and Weisman, L.S. (1998). The terminal tail region of a yeast myosin-V mediates its attachment to vacuole membranes and sites of polarized growth. Proc. Natl. Acad. Sci. USA **95,** 14799–14804.

Christensen, J.J. (1963). Corn smut caused by *Ustilago maydis*. Am. Phytopathol. Soc. Monogr. 2.

Garcia-Muse, T., Steinberg, G., and Perez-Martin, J. (2003). Pheromone-induced G(2) arrest in the phytopathogenic fungus *Ustilago maydis*. Eukaryot. Cell **2,** 494–500.

Gillissen, B., Bergemann, J., Sandmann, C., Schroeer, B., Bölker, M., and Kahmann, R. (1992). A two-component regulatory system for self/non-self recognition in *Ustilago maydis*. Cell **68,** 647–657.

Govindan, B., Bowser, R., and Novick, P. (1995). The role of Myo2, a yeast class V myosin, in vesicular transport. J. Cell Biol. **128,** 1055–1068.

Haarer, B.K., Petzold, A., Lillie, S.H., and Brown, S.S. (1994). Identification of MYO4, a second class V myosin gene in yeast. J. Cell Sci. **107**, 1055–1064.

Heath, I.B. (1995). The cytoskeleton. In The Growing Fungus, N.A.R. Gow and G.M. Gadd, eds (London: Chapman & Hall), pp. 99–134.

Hepler, P.K., Vidali, L., and Cheung, A.Y. (2001). Polarized cell growth in higher plants. Annu. Rev. Cell Dev. Biol. **17,** 159–187.

Hill, K.L., Catlett, N.L., and Weisman, L.S. (1996). Actin and myosin function in directed vacuole movement during cell division in *Saccharomyces cerevisiae*. J. Cell Biol. **135,** 1535–1549.

Holliday, R. (1974). *Ustilago maydis*. In Handbook of Genetics, R.C. King, ed (New York: Plenum Press), pp. 575–595.

Huang, J.D., Brady, S.T., Richards, B.W., Stenolen, D., Resau, J.H., Copeland, N.G., and Jenkins, N.A. (1999). Direct interaction of microtubule- and actin-based transport motors. Nature **397,** 267–270.

Johnston, G.C., Prendergast, J.A., and Singer, R.A. (1991). The *Saccharomyces cerevisiae* MYO2 gene encodes an essential myosin for vectorial transport of vesicles. J. Cell Biol. **113,** 539–551.

Kahmann, R., Romeis, T., Bölker, M., and Kamper, J. (1995). Control of mating and development in *Ustilago maydis*. Curr. Opin. Genet. Dev. **5,** 559–564.

Kämper, J., Reichmann, M., Romeis, T., Bölker, M., and Kahmann, R. (1995). Multiallelic recognition: Nonself-dependent dimerization of the bE and bW homeodomain proteins in *Ustilago maydis*. Cell **81,** 73–83.

Karcher, R.L., Roland, J.T., Zappacosta, F., Huddleston, M.J., Annan, R.S., Carr, S.A., and Gelfand, V.I. (2001). Cell cycle regulation of myosin-V by calcium/calmodulin-dependent protein kinase II. Science **293,** 1317–1320.

Karos, M., Chang, Y.C., McClelland, C.M., Clarke, D.L., Fu, J., Wickes, B.L., and Kwon-Chung, K.J. (2000). Mapping of the *Cryptococcus neoformans* MATα locus: Presence of mating type-specific mitogen-activated protein kinase cascade homologs. J. Bacteriol. **182,** 6222–6227.

Karpova, T.S., Reck-Peterson, S.L., Elkind, N.B., Mooseker, M.S., Novick, P.J., and Cooper, J.A. (2000). Role of actin and Myo2p in polarized secretion and growth of *Saccharomyces cerevisiae*. Mol. Biol. Cell **11,** 1727–1737.

Kumar, S., Tamura, K., Jakobsen, I.B., and Nei, M. (2001). MEGA2: Molecular evolutionary genetics analysis software. Bioinformatics **17,** 1244–1245.

Langford, G.M. (2002). Myosin-V, a versatile motor for short-range vesicle transport. Traffic **3,** 859–865.

Lehmler, C., Steinberg, G., Snetselaar, K.M., Schliwa, M., Kahmann, R., and Bölker, M. (1997). Identification of a motor protein required for filamentous growth in *Ustilago maydis*. EMBO J. **16,** 3464–3473.

Lengeler, K.B., Fox, D.S., Fraser, J.A., Allen, A., Forrester, K., Dietrich, F.S., and Heitman, J. (2002). Mating-type locus of *Cryptococcus neoformans*: A step in the evolution of sex chromosomes. Eukaryot. Cell **1,** 704–718.

Lillie, S.H., and Brown, S.S. (1994). Immunofluorescence localization of the unconventional myosin, Myo2p, and the putative kinesin-related protein, Smy1p, to the same regions of polarized growth in *Saccharomyces cerevisiae*. J. Cell Biol. **125,** 825–842.

McGoldrick, C.A., Gruver, C., and May, G.S. (1995). myoA of *Aspergillus nidulans* encodes an essential myosin I required for secretion and polarized growth. J. Cell Biol. **128,** 577–587.

Motegi, F., Arai, R., and Mabuchi, I. (2001). Identification of two type V myosins in fission yeast, one of which functions in polarized cell growth and moves rapidly in the cell. Mol. Biol. Cell **12,** 1367–1380.

Mulvihill, D.P., and Hyams, J.S. (2003). Role of the two type II myosins, Myo2 and Myp2, in cytokinetic actomyosin ring formation and function in fission yeast. Cell Motil. Cytoskeleton **54,** 208–216.

Oberholzer, U., Marcil, A., Leberer, E., Thomas, D.Y., and Whiteway, M. (2002). Myosin I is required for hypha formation in *Candida albicans*. Eukaryot. Cell **1,** 213–228.

Osherov, N., Yamashita, R.A., Chung, Y.S., and May, G.S. (1998). Structural requirements for in vivo myosin I function in *Aspergillus nidulans*. J. Biol. Chem. **273,** 27017–27025.

Plamann, M., Minke, P.F., Tinsley, J.H., and Bruno, K.S. (1994). Cytoplasmic dynein and actin-related protein Arp1 are required for normal nuclear distribution in filamentous fungi. J. Cell Biol. **127,** 139–149.

Rechsteiner, M. (1990). PEST sequences are signals for rapid intracellular proteolysis. Semin. Cell Biol. **1,** 433–440.

Reck-Peterson, S.L., Provance, D.W., Jr., Mooseker, M.S., and Mercer, J.A. (2000). Class V myosins. Biochim. Biophys. Acta **1496,** 36–51.

Riquelme, M., Gierz, G., and Bartnicki-Garcia, S. (2000). Dynein and dynactin deficiencies affect the formation and function of the Spitzenkorper and distort hyphal morphogenesis of *Neurospora crassa*. Microbiology **146**, 1743–1752.

Riquelme, M., Reynaga-Pena, C.G., Gierz, G., and Bartnicki-Garcia, S. (1998). What determines growth direction in fungal hyphae? Fungal Genet. Biol. **24,** 101–109.

Santos, B., and Snyder, M. (1997). Targeting of chitin synthase 3 to po-

larized growth sites in yeast requires Chs5p and Myo2p. J. Cell Biol. **136,** 95–110.

Schott, D., Ho, J., Pruyne, D., and Bretscher, A. (1999). The COOH-terminal domain of Myo2p, a yeast myosin V, has a direct role in secretory vesicle targeting. J. Cell Biol. **147,** 791–808.

Seiler, S., Nargang, F.E., Steinberg, G., and Schliwa, M. (1997). Kinesin is essential for cell morphogenesis and polarized secretion in *Neurospora crassa*. EMBO J. **16,** 3025–3034.

Shannon, K.B., and Li, R. (2000). A myosin light chain mediates the localization of the budding yeast IQGAP-like protein during contractile ring formation. Curr. Biol. **10,** 727–730.

Sietsma, J.H., Beth Din, A., Ziv, V., Sjollema, K.A., and Yarden, O. (1996). The localization of chitin synthase in membranous vesicles (chitosomes) in *Neurospora crassa*. Microbiology **142**, 1591–1596.

Snetselaar, K.M., Bölker, M., and Kahmann, R. (1996). *Ustilago maydis* mating hyphae orient their growth toward pheromone sources. Fungal Genet. Biol. **20,** 299–312.

Spellig, T., Bölker, M., Lottspeich, F., Frank, R.W., and Kahmann, R. (1994). Pheromones trigger filamentous growth in *Ustilago maydis*. EMBO J. **13,** 1620–1627.

Spellig, T., Bottin, A., and Kahmann, R. (1996). Green fluorescent protein (GFP) as a new vital marker in the phytopathogenic fungus *Ustilago maydis*. Mol. Gen. Genet. **252,** 503–509.

Steinberg, G. (2000). The cellular roles of molecular motors in fungi. Trends Microbiol. **8,** 162–168.

Steinberg, G., and Schliwa, M. (1995). The *Neurospora* organelle motor: A distant relative of conventional kinesin with unconventional properties. Mol. Biol. Cell **6,** 1605–1618.

Steinberg, G., Schliwa, M., Lehmler, C., Bölker, M., Kahmann, R., and McIntosh, J.R. (1998). Kinesin from the plant pathogen *Ustilago maydis* is involved in vacuole formation and cytoplasmic migration. J. Cell Sci. **111,** 2235–2246.

Straube, A., Brill, M., Oakley, B.R., Horio, T., and Steinberg, G. (2003). Microtubule organization requires cell cycle-dependent nucleation at dispersed cytoplasmic sites: Polar and perinuclear microtubule organizing centers in the plant pathogen *Ustilago maydis*. Mol. Biol. Cell **14,** 642–657.

Thompson, J.D., Gibson, T.J., Plewniak, F., Jeanmougin, F., and Higgins, D.G. (1997). The CLUSTAL_X Windows interface: Flexible strategies for multiple sequence alignment aided by quality analysis tools. Nucleic Acids Res. **25,** 4876–4882.

Urban, M., Kahmann, R., and Bölker, M. (1996). Identification of the pheromone response element in *Ustilago maydis*. Mol. Gen. Genet. **251,** 31–37.

Wedlich-Söldner, R., Bölker, M., Kahmann, R., and Steinberg, G. (2000). A putative endosomal t-SNARE links exo- and endocytosis in the phytopathogenic fungus *Ustilago maydis*. EMBO J. **19,** 1974–1986.

Wedlich-Söldner, R., Straube, A., Friedrich, M.W., and Steinberg, G. (2002). A balance of KIF1A-like kinesin and dynein organizes early endosomes in the fungus *Ustilago maydis*. EMBO J. **21,** 2946–2957.

Win, T.Z., Gachet, Y., Mulvihill, D.P., May, K.M., and Hyams, J.S. (2001). Two type V myosins with non-overlapping functions in the fission yeast *Schizosaccharomyces pombe*: Myo52 is concerned with growth polarity and cytokinesis, Myo51 is a component of the cytokinetic actin ring. J. Cell Sci. **114,** 69–79.

Woo, M., Lee, K., and Song, K. (2003). MYO2 is not essential for viability, but is required for polarized growth and dimorphic switches in *Candida albicans*. FEMS Microbiol. Lett. **218,** 195–202.

Xiang, X., Roghi, C., and Morris, N.R. (1995). Characterization and localization of the cytoplasmic dynein heavy chain in *Aspergillus nidulans*. Proc. Natl. Acad. Sci. USA **92,** 9890–9894.

Yamashita, R.A., and May, G.S. (1998). Constitutive activation of endocytosis by mutation of myoA, the myosin I gene of *Aspergillus nidulans*. J. Biol. Chem. **273,** 14644–14648.